Bulgarian Chemical Communications, Volume 55, Special Issue C (pp. 65–74) 2023 *DOI: 10.34049/bcc.55.C.0007*

Synthesis, crystallization region and structural peculiarities of the solid solutions in the Li_2MgGeO_4–Li_4GeO_4 system

V. V. Kostov-Kytin*, V. S. Nikolov*, N. V. Kuvandjiev

Institute of Mineralogy and Crystallography, Bulgarian Academy of Sciences, 1113 Sofia, "Akad. G. Bonchev" str., bl. 107

Received: November 2023; Revised: December 2023

Ten compositions of the system Li_2MgGeO_4-Li_4GeO_4 with general formula $Li_{2+2x}Mg_{1-x}GeO_4$ with x = 0–0.9 were studied. The syntheses were carried out by solid state reaction at 1050 °C. The X-ray diffractograms were analyzed with respect to crystallizing phases. It was established that all solid solutions contained an orthorhombic compound isostructural to γ-Li_3PO_4 being the only one or the main phase in all of the synthesized products. Rietveld refinement was applied in order to attain and evaluate certain structural parameters. A linear change of the lattice parameters and a decrease in cell volume were found with increasing Li content. Another clearly outlined dependence is that between the increasing content of lithium, respectively cation charge in the Li3 position and the decrease of approximately 8% in the volume of this cation octahedron. The obtained new results for the concentration region of these γ-type solid solutions as well as for their structural peculiarities can serve as a basis for their synthesis for various applications.

Keywords: oxides, chemical synthesis, phase equilibria, X-ray diffraction, crystal structure.

1. INTRODUCTION

Germanate compounds are widely used for various applications such as ceramics, optics, optoelectronics and lasers. Most of them are isostructural to the corresponding silicate compounds, but compared to the latter, they have lower melting temperatures, which facilitates their synthesis. Among the widely studied germanates are Zn_2GeO_4, Mg_2GeO_4, and Ca_2GeO_4. Mg_2GeO_4 and Zn_2GeO_4 have been tested as dielectric ceramics [1, 2] as well as phosphors after suitable doping by transition ions or rare earth ions for different emission in the visible region [3, 4]. The intermediate compounds of the systems Me_2GeO_4-Li_4GeO_4 (Me = Zn, Mg, Ca) i.e. Li_2ZnGeO_4, Li_2MgGeO_4, and Li_2CaGeO_4 have also been tested as dielectric ceramics [5, 6] and for phosphors [7–11]. Another promising application of these intermediates is as solid-state laser media doped with Cr^{4+} with a wide spectrum of radiation in the near infrared region (1.1–1.6 μm) [12, 13]. In this regard, much has been achieved in research on silicates of the Li_2MgSiO_4 type [14, 15]. Similar results would also be very likely for germanium structural analogues.

A particularly important area of the Me_2GeO_4-Li_4GeO_4 systems are the Li_2MeGeO_4-Li_4GeO_4 subsystems (where Me is Zn or Mg). After replacing of Me by Li in these subsystems, solid solutions with the general formula $Li_{2+2x}Me_{1-x}GeO_4$ crystallize. These solid solutions are isostructural to the orthorhombic γ-Li_3PO_4 and to the high-temperature modifications of Li_2ZnGeO_4 and Li_2MgGeO_4. Due to their specific structure, some of the Li ions are particularly mobile, which predetermines the high ionic conductivity of these solid solutions. The solutions are known as LISICON (lithium superionic conductors). Apart from their high conductivity, some of these solutions (according to the available data) are thermodynamically stable, i.e. unlike Li_2MeGeO_4, they do not show polymorphic transitions, which offers opportunities for single crystal growth (e.g. for solid-state lasers application).

Understanding the mechanism of the $Li_{2+2x}Me_{1-x}GeO_4$ materials ionic conductivity, as well as their potential for use in other applications, requires knowledge of the concentration and temperature regions of crystallization of these solid solutions,

* To whom all correspondence should be sent:
E-mails: vkytin@abv.bg; vnikolov@svr.igic.bas.bg

as well as of their crystal structures behavior upon changes in the Li/Me ratio. In reality, however, only the zinc form (Me = Zn) – $Li_{2+2x}Zn_{1-x}GeO_4$ solid solutions have been studied in detail to date.

The regions of existence of the γ-Li_3PO_4-type $Li_{2+2x}Zn_{1-x}GeO_4$ as well as their crystal structures have been well studied mainly with emphasis on their ionic conductivity. According to the research of Bruce and West [16] $Li_{2+2x}Zn_{1-x}GeO_4$ region is localized from x = 0.20 to x = 0.85 at 1000 °C. At 600 °C the region narrows from x = 0.35 to x = 0.73. Its crystal structure has been determined by H. Hong [17] using single crystal X-ray analysis (Pnma, a = 10.828 Å, b = 6.251 Å, c = 5.140 Å, z = l). The structure has been described as built up by isolated GeO_4 tetrahedra linked to two crystallographic types of mixed (Li, Zn)O_4 tetrahedra in a way to form a rigid three-dimensional network of $Li_{II}Zn(GeO_4)_4$ (Fig. 1a). The three remaining Li^+ ions in $Li_{14}Zn(GeO_4)_4$ have occupancies of 55 and 16%, respectively, at the 4c and 4a interstitial positions (designated Li3 and Li4 in Fig 1a).

In 1979 Plattner &Voellenkle [18] determined by X-ray diffraction the crystal structure of $Li_3Zn_{0.5}GeO_4$ (Pmnb, a = 6.29, b = 10.74, c = 5.17 Å). Although these authors have confirmed its structural identity with Hong's phase (the basic framework of Ge, (Li, Zn), and O atoms is very similar in both refinements) they have failed to identify the existence of one of the eight-fold lithium sites – that one designated as Li4 in Fig 1a (vs. Fig. 1b). The relatively weak X-ray scattering factors for lithium ions puts certain limitations to the X-ray diffraction technique when accurate lithium-ion distributions are required. In 1988 Abrahams *et al*. used powder neutron diffraction patterns obtained at a constant wavelength to solve the crystal structures of two LISICON compounds with formulae $Li_3Zn_{0.5}GeO_4$ and $Li_{3.5}Zn_{0.25}GeO_4$, correspondingly [19]. In 1989 Abrahams *et al*. applied high resolution powder neutron diffraction and re-examined the structure of the former compound [20]. These authors overcome the shortcomings of X-ray diffraction and drew new light on the lithium distribution in the crystal structures of these materials. Thus, the authors: (i) confirmed the location of lithium in the Li4 site; (ii) moved off the Li(3) ion from the special position onto an eightfold general position; (iii) well determined the lithium positions in sites (2) and (2a) (Fig 1c). Abrahams *et al*. [20] also paid attention to the fact that the structures of these lithium ion conductors can be derived from that one of the stoichiometric parent g-Li_2ZnGeO_4 compound, by $Zn^{2+}\rightarrow 2Li^+$ substitution. Thus, while some of the Li atoms substitute for the Zn^{2+} ion in a tetrahedral site – Li1 or Li2 the excess Li atoms occupy any one of the two octahedral interstitial sites – Li3 or Li4 (Fig. 1).

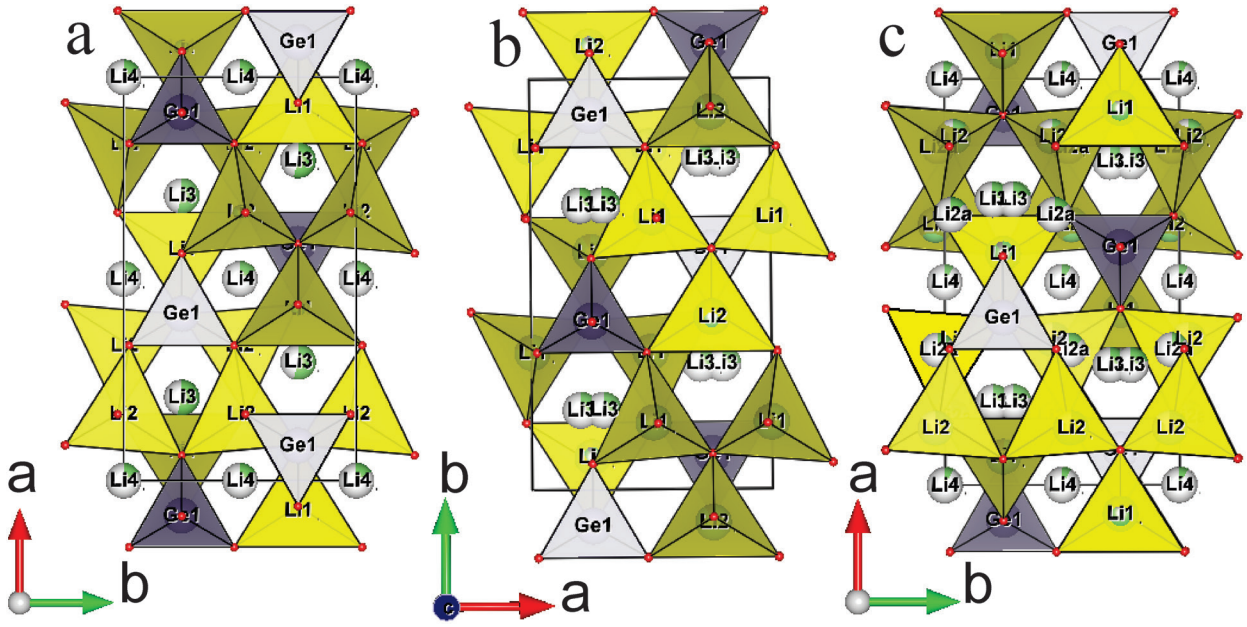

Fig. 1. Crystal structures of $Li_{2+2x}Zn_{1-x}GeO_4$ solid solutions a) $Li_{14}Zn(GeO_4)_4$ (Hong, 1978 – [17]); b) $Li_3Zn_{0.5}GeO_4$ (Plattner &Voellenkle, 1979 – [18]); c) $Li_3Zn_{0.5}GeO_4$ (Abrahams *et al*., 1989 – [20]).

The essential structural feature of the LISICONs is a rigid, three-dimensional network having partially occupied by lithium ions sites linked in a three dimensional interstitial space ensuring fast ion transfer from an occupied interstitial position to a neighboring empty one [21]. For fast Li^+ ion transport, the Li-O polyhedra around adjacent Li^+ positions must share a common face. The smallest diameter of such faces, which act as bottlenecks to ion motion, should be greater than twice the sum of the alkali-ion and oxygen-ion radii. Thus for fast Li^+-ion transport the smallest diameter should exceed 4.32 Å since the radii of the Li^+ and O^{2-} ions are respectively 0.76 and 1.4 Å [22]. In 1977 Hong postulated that in addition to these geometrical constraints, chemical bonding also plays a role in determining alkali ions (A^+) mobility in solid electrolytes [21]. One of the newly noted key features resulting in fast Li-ion conduction for certain lithium super ionic conductors "is the enlarged Li site given by large local space of crystal structures promoting Li disordering." In 2019 He *et al*. established that "the enlarged Li site corresponds to a large local space larger than 2.4 Å in size and can be occupied by Li ion at multiple positions within a very close distance. Li ions move rapidly within the enlarged site, in contrast to thermal vibration centered to the equilibrium positions of a regular site." [23].

The crystal structures of the two most thoroughly researched solid solutions – $Li_3Zn_{0.5}GeO_4$ and $Li_{3.5}Zn_{0.25}GeO_4$, determined by powder neutron diffraction studies as mentioned above provide good evidence for such enlarged sites in which multiple partially-occupied close-neighboring lithium ions with relatively high values of their atomic displacement parameters have been established [19, 20].

In contrast to $Li_{2+2x}Zn_{1-x}GeO_4$ the solid solutions $Li_{2+2x}Mg_{1-x}GeO_4$, have been investigated too insufficiently. In 1971, West et al. established the existence of 4 polymorphic modifications of Li_2MgGeO_4 among which the high-temperature γ-form was found to be isostructural to γ Li_3PO_4 [24]. These modifications were also confirmed by Monnaye et al. and Monnaye [25, 26]. In 2013, Nakayama et al. studied in detail the structural features of the low-temperature modifications and the conditions for transitions between them and to the γ-modification [27]. Only Hong [17] had studied the solid solutions with compositions $Li_{16-2x}D_x(TO_4)_4$, with D = Mg or Zn, T = Si or Ge, and declaring $0<x<4$. The latter formula can also be represented as $Li_{2+2x}D_{1-x}TO_4$ ($0<x<1$) as more suitable for cases where the emphasis of research falls on the substitution of D(Me) elements by lithium. Such an approach is also adopted in the present work. In Hong's work, however, there is no specifics about crystallization regions of the solid solutions, data on the conductivity of only three discrete compositions, namely $Li_{2.5}Mg_{0.75}GeO_4$, $Li_3Mg_{0.5}GeO_4$, and $Li_{3.5}Mg_{0.25}GeO_4$ (x = 0.25; 0.5; 0.75, correspondingly) and the crystal structure of only the zinc analogue of $Li_{3.5}Mg_{0.25}GeO_4$ is presented.

This study presents the results of research on the synthesis conditions, crystallization region and structural characterization of the $Li_{2+2x}Mg_{1-x}GeO_4$ solid solutions from Li_2MgGeO_4 to Li_4GeO_4. Conventional powder X-ray diffraction (CPXRD) was used to characterize the obtained materials. This method does not have the capabilities of other diffraction methods for precise determinations of lithium in terms of its structural positions and occupancy. In this study, however, CPXRD was applied to samples comprising a compositional series. This makes it possible to derive important trends and dependencies related to the crystal-chemical characteristics and behavior of the studied materials, regardless of the noted limitations of the method and the lack of a reliably determined chemical composition.

2. SYNTHESIS AND STRUCTURAL STUDIES

2.1. Synthesis of solid solutions

Due to the lack of data on the region of solid solution crystallization, a study of the entire region of the Li_2MgGeO_4 – Li_4GeO_4 system was planned. A series of $Li_{2+2x}Mg_{1-x}GeO_4$ solid solutions with x = 0, 0.1, 0.2, 0.3, 0.4, 0.5, 0.6, 0.7, 0.8 and 0.9 were synthesized by the solid state method, i.e. the composition of $Li_{2+2x}Mg_{1-x}GeO_4$ was varied from Li_2MgGeO_4 to $Li_{3.8}Mg_{0.1}GeO_4$. Solid phase method was applied as Bruce and West [16] did it. Li_2CO_3 with a purity of 99.9%, MgO with a purity of 99.99% and GeO_2 with a purity of 99.999% were used as starting reagents. Before synthesis, Li_2CO_3 and GeO_2 were dried to a constant weight at 150 °C for 5 hours. MgO was heat treated at 700 °C for 5 hours to convert available amounts of $Mg(OH)_2$ back to MgO. It was found that the starting reagent MgO contains up to 3% $Mg(OH)_2$, which is completely converted into MgO during the treatment. This was confirmed with relevant X-ray and DTA analyses. Weighed with an accuracy of 0.001 g, the starting reagents with a total weight of 4 g were mixed and crushed in an agate

mortar. Synthesis was carried out in a Kanthal resistance furnace with a temperature controller-programmer type Eurotherm 2704. A coated platinum crucible 3×3 cm was used. The samples were decarbonized at 800 °C for 3 hours. The tests showed that under these conditions Li_2CO_3 was completely decarbonized. After a new grinding the samples were heated at 1050 °C for 16 h with double intermediate grinding. Preliminary experiments have shown that this is the optimal temperature for solid-state synthesis to maximally limit the vaporization of components and to obtain as pure as possible final product. The samples were quenched directly from the furnace, i.e. their cooling to 100 °C took 2–3 minutes. The tests after the final synthesis showed that the residual amount corresponds exactly to the theoretical one, i.e. no evaporation losses of components were detected.

2.2. Methods for structural characterization

2.2.1. Powder X-ray diffraction

The diffraction patterns of all samples were collected at room temperature on an Empyrean (MalvernPanalytical) powder X-ray diffractometer, equipped with a multichannel PIXcel3D detector, using HDD Cu Kα (λ = 0.154060 nm) radiation, at 40 kV and 30 mA, in the range 5–80° 2θ and a scan step of 0.013° counting time (s): 23.97 (total time appx. 10 minutes).

2.2.2. Phase identification and choice of starting structural models

The crystal structure of $Li_3Zn_{0.5}GeO_4$ (ICSD #65643; [20]) as determined by Abrahams *et al*., in 1989 was used as an initial structural model for further investigations of the main $Li_{2+2x}Mg_{1-x}GeO_4$ phases (Fig. 1c). Certain replacements and amendments were made in the CIF file in consistency with the compositions of the initial synthesis batches as well as with the limitation of the used X-ray technique for detection of the weak scattering lithium ions as follows:

(i) Zn was replaced by Mg;

(ii) The total occupancy of the mixed tetrahedrally coordinated (Li,Mg) sites was fixed at one;

(iii) The total magnesium content in any of the investigated structures was set to be equal to that one put in the initial synthesis batch and further on it was divided between the two mixed tetrahedrally coordinated (Li/Mg) positions in a ratio of approx. 1:2 (atomic positions Li1 and Li2 in Fig. 1). The occupancies of these positions were subsequently included in the refinement;

(iv) Li(2a) position (Fig. 1c) was omitted from the refinement;

(v) The excess Li atoms in amounts derived from those ones set in the initial batches extracting the lithium from the mixed (Li/Mg) positions were distributed between the two octahedral interstitial sites – Li3 and Li4 randomly but always the occupancy of Li3 at least twice as bigger as that one of Li4. The occupancies of these positions were not included in the refinement procedure;

(vi) Li3 was fixed in the special position x,1/4/,0;

2.2.3. Rietveld Refinements

Ten samples of crystalline samples prepared at 1050 °C from initial batches with various Li/Mg ratios have been studied. The Rietveld refinement procedures were carried out with the GSAS-EXPGUI suite of programs (Larson, Von Dreele, 2004; Toby, 2001) [28, 29]. The Bragg peak profile was modelled using a pseudo-Voigt function; the background curve was fitted using a Chebyshev polynomial with 12 variable coefficients. The scattering curves of neutral atoms, as stored in GSAS, were used. No corrections were made for absorption. All of the atomic thermal displacement parameters were refined isotropically. Expecting similar U_{iso} values for the O atoms, these were refined in a group. The Li and Mg ions in both mixed tetrahedrally coordinated positions of the title compounds were constrained in terms of x, y, z, U_{iso}, and occupancy. Soft constraints (restraints) were imposed on the Ge-O distances. One and the same Restraint Weighting factor (RWf) fixed at 10,000 was used throughout the refinement procedure.

2.2.4. Visualization and geometric parameters calculations

The following programs have been used for graphic presentations:

1. WinPLOTR utilities ver. June 2020 (Thierry Roisnel, Rennes, France) as a Windows tool [30] (powder X-ray diffraction patterns);

2. VESTA ver. 3.3.2 (Koichi Momma, Tsukuba, Japan) [31] for visualization of certain structure and topological motives. The program has also been used for calculation of various geometric parameters such as the average bond lengths between the central atom and its ligands in a coordination polyhedron (abl) and the polyhedral volume (PV) of any cation in the structure.

3. RESULTS

Ten compositions were synthesized in the system Li_2MgGeO_4-Li_4GeO_4 with general formula $Li_{2+2x}Mg_{1-x}GeO_4$ with x = 0–0.9 i.e. from Li_2MgGeO_4 to $Li_{3.8}Mg_{0.1}GeO_4$ and designated hereinafter as Li2Mg, Li2.2Mg0.9, Li2.4Mg0.8, Li2.6Mg0.7, Li2.8Mg0.6, etc.

Initial inspection of the powder X-ray diffraction data as well as the conducted phase identification have revealed that all of the studied samples consist of well crystallized run-products. In all cases the orthorhombic $Li_{2+2x}Mg_{1-x}GeO_4$ is the predominant phase and it is the only one detected in samples $Li_{3.0}Mg_{0.5}GeO_4$, $Li_{3.2}Mg_{0.4}GeO_4$, $Li_{3.4}Mg_{0.3}GeO_4$, and in $Li_{3.8}Mg_{0.1}GeO_4$. Among the concomitant compounds only two have reliably been identified. One of them is the Mg-substituted structural analogue of the monoclinic Li_2ZnGeO_4 (ICSD #34362; [32]). It has occurred in the $Li_{2.0}Mg_{1.0}GeO_4$ (37.0 weight %) and $Li_{2.2}Mg_{0.9}GeO_4$ (26.0 weight %) samples and traces of it could be detected in $Li_{2.4}Mg_{0.8}GeO_4$. The other compound is the monoclinic Li_2GeO_3. (ICSD #100403; [33] which has been detected as a run-product in an amount of about 2 wt% in only one sample – $Li_{2.8}Mg_{0.6}GeO_4$. Other small quantity of unidentified crystalline phases has been detected in the following samples: $Li_{2.0}Mg_{1.0}GeO_4$; $Li_{2.2}Mg_{0.9}GeO_4$; $Li_{2.4}Mg_{0.8}GeO_4$, $Li_{2.6}Mg_{0.7}GeO_4$, and $Li_{3.6}Mg_{0.2}GeO_4$. Subsequently, these have been excluded from the Rietveld refinement procedures which definitely has affected the results of the quantitative analyses but has not impacted determination and evaluation of the main phase crystal chemical peculiarities.

Figure 2 presents PXRD patterns of selected $Li_{2+2x}Mg_{1-x}GeO_4$ with some of the concomitant phases designated therein.

Figure 3 presents Rietveld refinement plot for the $Li_{3.0}Mg_{0.5}GeO_4$ solid solution.

Table 1 presents lattice parameters and refinement details for selected $Li_{2+2x}Mg_{1-x}GeO_4$ solid solutions.

As can be seen from Table 1 with increase of the Li contents into the $Li_{2+2x}Mg_{1-x}GeO_4$ solid solution the lattice parameters *a* and *b* progressively decrease whereas the parameter *c* increases resulting in the lattice volume decrease, after all.

Table 2 presents positional and thermal parameters of atoms in the structure of (sample Li2.8Mg0.6) as obtained from the PXRD studies using Restraint Weighting factor.

Table 3 presents selected geometric parameters measured to characterize the crystal structural peculiarities of $Li_{2+2x}Mg_{1-x}GeO_4$ solid solution.

Figures 4 presents variations of lattice parameters (*a*, *b*, *c*, *V*) and Figure 5 – the relationship be-

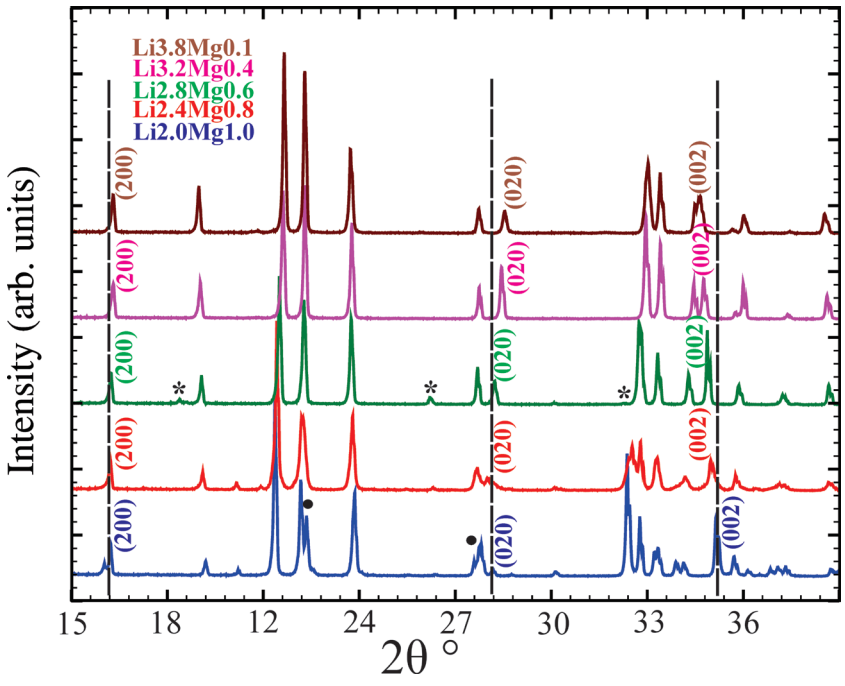

Fig. 2. PXRD patterns of selected $Li_{2+2x}Mg_{1-x}GeO_4$ with some of the concomitant phases designated: • – the monoclinic Li_2MgGeO_4 [32]; ∗ – monoclinic Li_2GeO_3 [33].

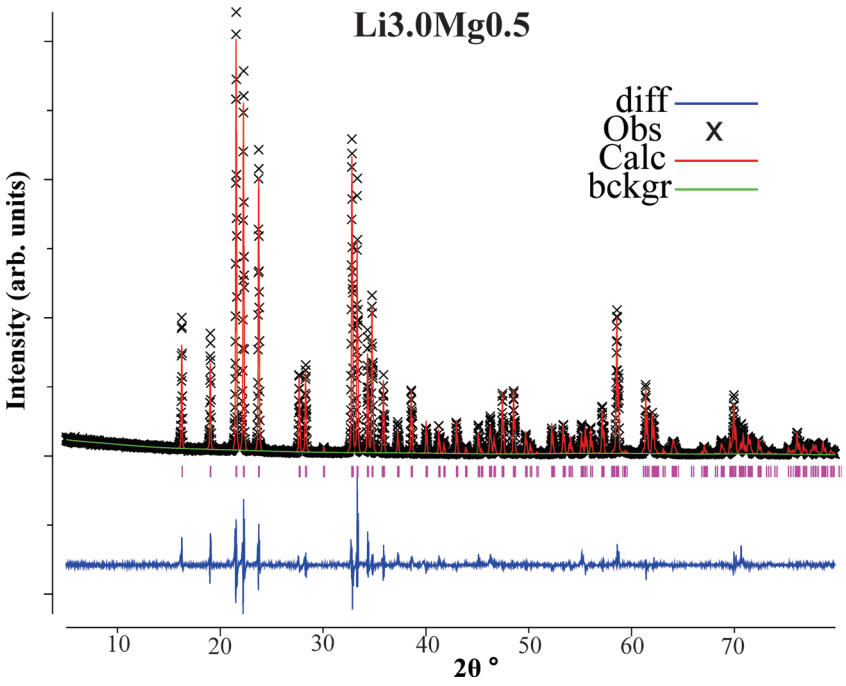

Fig. 3. Rietveld refinement plot for a $Li_{3.0}Mg_{0.5}GeO_4$ solid solution showing experimental data (x), calculated diffraction profile (red curved line), difference curve between experimental and calculated values (solid blue curve at the bottom), background (green line), and calculated Bragg positions of α1 and α2 reflections (small bars above the difference curve).

Table 1. Lattice parameters and refinement details for selected $Li_{2+2x}Mg_{1-x}GeO_4$ solid solution

	Powder X-ray diffraction studies (selected samples):				
	Li2.2Mg0.9 Two phase study	Li2.6Mg0.7 Single phase study	Li3.0Mg0.5 Single phase study	Li3.4Mg0.3 Single phase study	Li3.8Mg0.1 Single phase study
	1	*2*	*3*	*4*	*5*
Space Group, Z	*Pnma, 4*	*Pnma, 4*	*Pnma, 4*	*Pnma, 4*	*Pnma, 4*
a (Å)	10.9475(6)	10.9275(3)	10.9070(2)	10.8968(2)	10.8870(2)
b (Å)	6.4068(4)	6.3540(3)	6.3062(1)	6.2996(1)	6.2611(2)
c (Å)	5.1217(2)	5.1402(2)	5.15990(8)	5.17144(8)	5.1808(1)
V (Å)^3	359.23(4)	356.90(3)	354.9(1)	355.00(1)	353.15(2)
Rwp (%)	18.56	16.34	17.45	16.11	16.48
Rp (%)	13.29	12.38	13.12	11.99	12.32
Red-χ^2	5.966	4.339	5.065	3.553	4.43
N_{obs}	480	252	247	250	249
RF (%)	5.12	4.42	6.29	5.39	6.79
N_{var}	72	48	54	56	57
Number of restraints	4	4	4	4	4
Total restraint χ^2 contribution	40.40	39.30	95.16	4.25	6.15

tween the polyhedral volume of Li3 in its octahedrally coordinated position with the initial lithium content used for the preparation of the studied solid solution compounds. Trend-lines, linear equations and R-squared values are also depicted.

4. DISCUSSION

The presence of the monoclinic Li_2MgGeO_4 among the run products of the syntheses yielding samples with low lithium content (e.g. in $Li_{2.0}Mg_{1.0}$

Table 2. Positional and thermal parameters of atoms in the structure of the Li2.8Mg0.6 sample

Atom	x	y	z	Sof	$100xU_{iso}$,
Ge	0.4142(2)	0.25	0.3297(3)	1	2.56(5)
O1	0.3352(7)	0.0253(7)	0.219(1)	1	3.4(1)
O2	0.0838(9)	0.75	0.167(1)	1	3.4(1)
O3	0.0651(6)	0.25	0.269(1)	1	3.4(1)
Li1	0.426(2)	0.75	0.161(4	0.86	5.4(4)
Mg1	0.426(2)	0.75	0.161(4)	0.14	5.4(4)
Li2	0.168(1)	-0.003(1)	0.307(2)	0.78	2.8(2)
Mg2	0.168(1)	-0.003(1)	0.307(2)	0.22	2.8(2)
Li3	0.204(0)	0.25	0.00	0.16	0.09
Li4	0.00	0.00	0.5	0.08	0.09

Table 3. Selected geometric parameters measured to characterize the crystal structural peculiarities $Li_{2+2x}Mg_{1-x}GeO_4$ solid solution

	GeO tetrahedron		Li1O tetrahedron		Li3O octahedron		Li4O octahedron	
Samples	abl, Å	PV, A^3	abl, Å	PV, A^3	abl, Å	PV, A^3	abl, Å	PV, A^3
Li2.0Mg1.0	1.7317	2.6555	2.0163	3.9768	2.3981	17.0408	2.2344	14.6406
Li2.2Mg0.9	1.7348	2.6618	2.0325	3.8798	2.3987	17.2181	2.2227	14.4034
Li2.4Mg0.8	1.7414	2.7092	2.0317	3.9019	2.3884	16.9592	2.2222	14.3892
Li2.6Mg0.7	1.7434	2.7164	2.0328	4.0223	2.3703	16.6143	2.241	14.7893
Li2.8Mg0.6	1.7439	2.7166	2.0026	4.0218	2.3614	16.4867	2.246	14.9134
Li3.0Mg0.5	1.7411	2.703	2.0091	3.9877	2.3668	16.5384	2.2291	14.5685
Li3.2Mg0.4	1.7623	2.8065	1.9938	3.9358	2.3463	16.2056	2.235	14.7248
Li3.4Mg0.3	1.7561	2.7741	2.0047	3.8534	2.3707	16.6049	2.21	14.3578
Li3.6Mg0.2	1.7436	2.6953	2.0321	4.2327	2.3366	15.9241	2.2739	15.4935
Li3.8Mg0.1	1.7454	2.7271	1.9916	3.9862	2.3517	16.3209	2.2257	14.4926

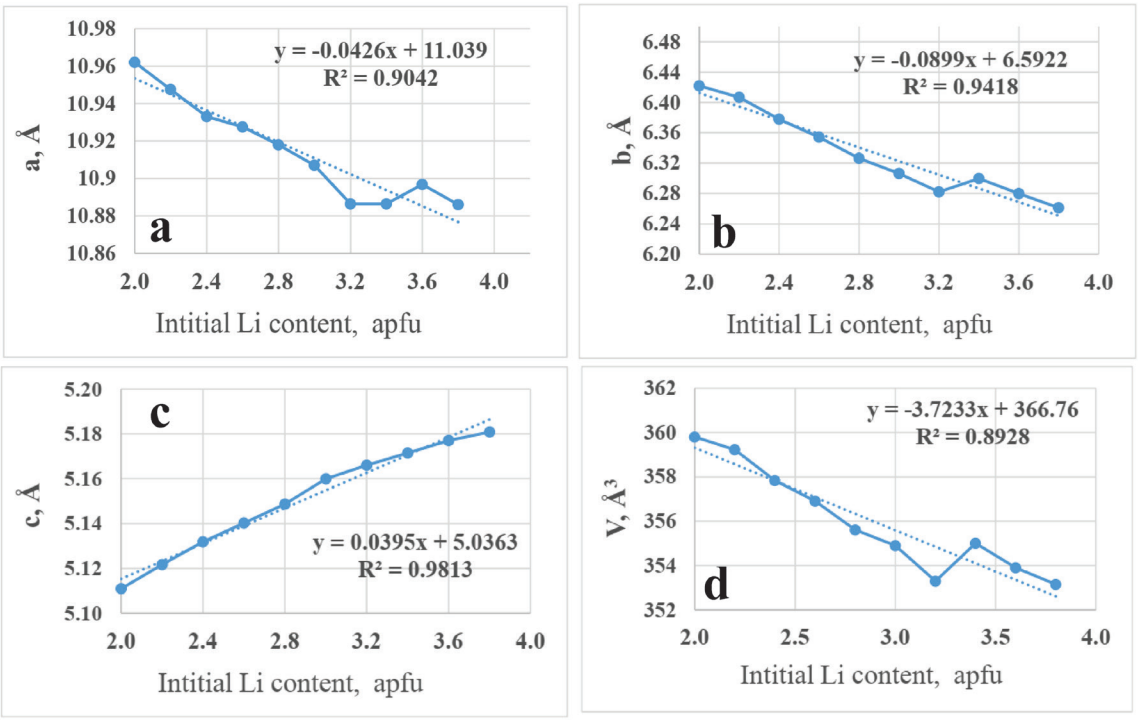

Fig. 4. Variations of lattice parameters (*a*, *b*, *c*, *V*) with initial lithium content for the studied $Li_{2+2x}Mg_{1-x}GeO_4$ solid solutions. The linear trend-lines are depicted as dotted lines.

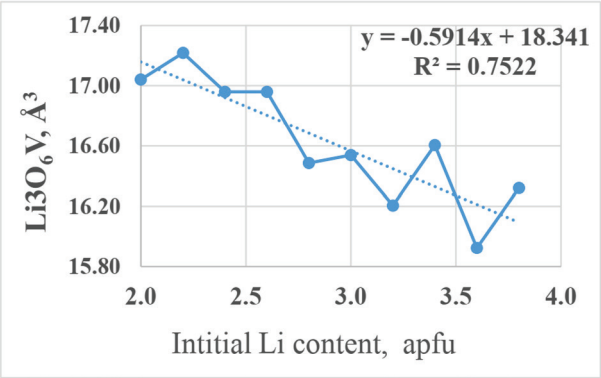

Fig. 5. Relationship between the polyhedral volume of Li3 in its octahedrally coordinated position with the initial lithium content. The linear trend-line is depicted as a dotted line.

– 37 wt %; $Li_{2.2}Mg_{0.9}$ – 26 wt %, and possibly in $Li_{2.4}Mg_{0.8}$; see Supplementary materials) is more or less expected in view of the earlier observations of researchers conducting experiments in a similar system to the one studied here and under similar synthesis conditions. The presence of the monoclinic modification is assumed to be due to the already established polymorphic transitions of Li_2ZnGeO_4 and Li_2MgGeO_4 [16, 34]. The other contaminations do not follow any trends and regularities, both quantitatively and in terms of their structural type. This means that the studied system is very sensitive to any fluctuations in the synthesis conditions and is alternatively also affected by post-synthesis treatment and thermodynamic stability of the end products. In this regard, previous investigation of the $Li_{2+2x}Zn_{1-x}GeO_4$ solid solutions showed that a couple of processes could have occurred at lower temperature such as: polymorph transition, precipitation, transformation of the γ-structure to another γ-substructure as well as the "aging" effect which nature is not entirely clarified, yet [34].

In four out of a total of ten examined $Li_{2+2x}Me_{1-x}GeO_4$ samples the orthorhombic phase is the only registered phase (Table 1, and Figures 2 and 3). In another four cases, the concomitant phases are around and below 4 wt.% of the total amount. Where unidentified phases are present in the final products this inevitably affects the data obtained from the quantitative analysis and the results can only be used as a guide. Additionally, the limitations of the applied diffraction method have led to certain simplification of the initial structural models used to refine the crystal structures of $Li_{2+2x}Me_{1-x}GeO_4$, which subsequently has degraded the values for some of the obtained R-factors (Table 1). In summary, all these shortcomings undoubtedly have affected the reliability of the data concerning the geometric parameters measured in order to characterize the crystal structural peculiarities of $Li_{2+2x}Me_{1-x}GeO_4$ of the studied samples (Table 3; Supplementary materials), especially since there is a lack of specific data on the chemical composition of the main phase.

Regardless of the fluctuations in many of the observed values, some of them exhibit certain trends depending on the initially set amount of lithium in the synthesis batches. It was found in this study that at 1050 °C the range $Li_{2+2x}Mg_{1-x}GeO_4$ exists between x = 0.15 and x = 0.9. In comparison with the solid solutions $Li_{2+2x}Zn_{1-x}GeO_4$ this range is a little wider.

It is worth noting that the volume of the measured unit cells decreases with increasing Li content about 1.7% (Table 1, Figure 4d), accompanied at the same time by a decrease in the values of *a* and *b* lattice parameters, but with an increase in *c*-dimensions (Figure 4 a–c). Moreover, the correlation coefficient between values of the *c*-parameter and initial lithium content is so high that in future investigations this dependence could easily be used for fast chemical composition determination of the studied compounds according to Vegard's rule, for example. The decreases of the unit cells by the increase of the Li content could not be explained taking into account only the ionic differences of Li^{2+} and Mg^{2+} in fourth coordination (0.59 for Li and 0.57 for Mg) [22]. For the zinc form – $Li_{2+2x}Zn_{1-x}Geo_4$ the cell volume decreases slightly too when the Li content increase (atomic radius of 0.6 for Zn). [16, 22]. It seems likely that inner electrostatic interactions predetermine such shrinkage.

Another clearly outlined dependence is that one between the increasing content of lithium in the Li3 position and the decrease in the volume of the octahedrally coordinated polyhedron it occupies there (approx. 8% within the studied compositional range). A plausible reason for this is the ever-increasing electrostatic attraction between the increasing in number lithium cations populating the central part of the octahedral-shaped interstitium in this part of the structure (increase in positive charge) and the surrounding ligands (oxygens). The average bond length in the polyhedron changes from 2.40 Å to 2.34 Å or about 2.5% in the studied compositional range (Table 3, column 9). The dimensions are comparable to those reported by He et al. in 2019 [24] to ensure concerted migration of the Li ions. Along with this, however, it is quite possible that such volume shrinkage

may lead to reduction of the number of multiple partially-occupied close-neighboring lithium sites and further to cause their unification in common positions, which will inevitably affect the values of the activation energy needed to facilitate Li-ion diffusion through the structure. To the best of our knowledge this is the first experimentally supported evidence for such structural shrinkage and the possible consequences.

5. CONCLUSION

This study establishes for the first time that the $Li_{2+2x}Mg_{1-x}GeO_4$ solid solutions exist within wide limits, just like the corresponding $Li_{2+2x}Zn_{1-x}GeO_4$ solid solutions. The presence of small amounts of concomitant phases among the run-products could be due to polymorphic transitions for compositions of x from 0 to 0.2 or occur probably due to interactions with the atmosphere or as a result of small transformations of the γ-phase to other γ-modifications at lower temperatures for the rest of the compositions. Similar transformations at low temperatures, resulting in a sharp reduce in the ionic conductivity, have previously been described for some $Li_{2+2x}Zn_{1-x}GeO_4$ solid solutions and undoubtedly necessitate further research. Regardless of the presence of by-phases, certain trends were found in some of the structural parameters of the synthesized $Li_{2+2x}Mg_{1-x}GeO_4$ with a change in the Li/Mg ratio. The volume of the measured unit cells decreases with increasing Li content accompanied at the same time by a decrease in the values of *a* and *b* lattice parameters, but with an increase in *c*-dimensions. Moreover, the correlation coefficient between values of the *c*-parameter and initial lithium content is very high (Vegard's low).

Another clearly outlined dependence is that, between the increasing content of lithium in the Li3 position and the decrease in the volume of the octahedrally coordinated polyhedron Li occupies there (approx. 8%). Undoubtedly, changes in the structural parameters of $Li_{2+2x}Mg_{1-x}GeO_4$ solid solutions with a change in the Li/Mg ratio will have an impact on the properties of solid solutions ceramics as ion conductivity, dielectric permittivity, and phosphor or laser emission after doping.

Acknowledgements: *The authors acknowledge the technical support from the project PERIMED BG- 05M2OP001-1.002-0005 /29.03.2018 (2018–2023).*

REFERENCES

1. J. Chen, Y. Tang, C. Yin, M. Yu, H. Xiang, C. Li, X. Xing, L. Fang, *JACerS*, **103**(3), 1789 (2020). https://doi.org/10.1111/jace.16855.
2. S. Wu, Q. Ma, *J. Alloys Compd*., **567**, 40 (2013). https://doi.org/10.1016/j.jallcom.2013.03.052.
3. H. M. Yang, J. Shi, M. L. Gong, H. Liang, *Mater. Lett.*, **64**, 1034 (2010). https://doi.org/:10.1016/j.matlet.2010.02.001.
4. H. M. Yang, Z. Wang, M. L. Gong, H. Liang, *J. Alloys Compd.*, **488**(1), 331 (2009). https://doi.org/10.1016/j.jallcom.2009.08.123.
5. C. Li, H. Xiang, M. Xu, Y. Tang, L. Fang, *J. Eur. Ceram. Soc.*, **38**(4), 1524 (2018). https://doi.org/10.1016/j.jeurceramsoc.2017.12.038.
6. J. I. Viegasa, R. L. Moreira, A. Diasa, *Vib. Spectrosc.*, **110**, 103 (2020). https://doi.org/10.1016/j.vibspec.2020.103130.
7. Y. Jin, Y. Hu,. *Mater. Res. Bull.*, **61**, 16 (2014). http://dx.doi.org/10.1016/j.materresbull.2014.09.085.
8. V. Berezovskaya, N. P. Efryushin, I. I. Seifullin, E. E. Martsinko, B. I. Zadneprovski ,G. B. Stryganyuk, A. S. Voloshinovskii, S. M. Levshov, V. P. Dotsenko, *Ceram. Int.*, **39**, 6835 (2013). https://doi.org/10.1016/j.ceramint.2013.02.015.
9. R. Cao, D. Ceng, X. Yu, S. Guo, Y. Wen, G. Zheng, *Funct. Mater. Lett.*, **8**(5), 1550046 (2015). https://doi.org/10.1142/S1793604715500460.
10. N. Bednarska-Adam, M. Kuwik, E. Pietrasik, W. A. Pisarski, T. Goryczka, B. Macalik, J. Pisarska, *Materials*, **15**, 5263 (2023). https://doi.org/10.3390/ma15155263.
11. Y. Jin, Y. Hu, H. Duan, L. Chen, X. Wang, *RSC Adv.*, **4**(22), 11360 (2014). https://doi.org/10.1039/C3RA47760F.
12. C. Li, J. Xu, W. Liu, D. Zheng, S. Zhang, Y. Zhang, H. Lin, L. Liu, J. Liu, F. Zeng, *J. Alloys Compd.*, **636**, 211 (2015). http://dx.doi.org/10.1016/j.jallcom.2015.02.121.
13. D. Wang, X. Zhang, X. Wang, Z. Leng, Q. Yang, W. Ji, H. Lin, F. Zeng, C. Li, Z. Su, *Crystals*, **10**(11), 1019 (2020). https://doi.org/10.3390/cryst10111019.
14. C. Jousseaume, A. Kahn-Harari, J. Derouet, D. Vivien, in: Advanced Solid-State Lasers, (M. Fermann and L. Marshall, eds.), 68 of Trends in Optics and Photonics Series (Optica Publishing Group, 2002), paper TuB 12. https://doi.org/10.1364/ASSL.2002.TuB12.
15. C. Anino, J. Thery, D. Vivien, in: Advanced Solid State Lasers (ASSL) p. SC6). Optica Publishing Group (1997). https://doi.org/10.1364/ASSL.1997.SC6.
16. P. G. Bruce, A. R. West, *Mater. Res. Bull.*, **15**(3), 379 (1980). https://doi.org/10.1016/0025-5408(80)90182-8.
17. H. P. Hong, 1978. *Mater. Res. Bull.*, **13**(2), 117 (1978). https://doi.org/10.1016/0025-5408(78)90075-2.
18. E. Plattner, H. Völlenkle, *Monatsh. Chem.*, **110**, 693 (1979). https://doi.org/10.1007/BF00938373.
19. I. Abrahams, P. G. Bruce, A. R. West, W. I. F. David, *J. Solid State Chem.*, **75**(2), 390 (1988). https://doi.org/10.1016/0022-4596(88)90179-X.

20. I. Abrahams, P. G. Bruce, W. I. F. David, A. R. West, *Acta Crystallogr. B*, **45**(5), 457 (1989). https://doi.org/10.1107/S0108768189006245.
21. H. Y-P. Hong, Chapter 10. New Solid Electrolytes, in: Solid State Chemistry of Energy Conversion and Storage, June 1, 179 (1977). https://doi.org/10.1021/ba-1977-0163.ch010.
22. R. D. Shannon, *Acta Crystallogr. A*. **32** (5), 751 (1976). https://doi.org/10.1107/S0567739476001551.
23. X. He, Q. Bai, Y. Liu, A. M. Nolan, C. Ling, Y. Mo, *Adv Energy Mater.*, **9**(43), 1902078 (2019). https://doi.org/10.1002/aenm.201902078.
24. A. R. West, F. P. Glasser, *J. Mater. Sci.*, **6**, 1100 (1971). https://doi.org/10.1007/BF00980609.
25. B. Monnaye, C. Garrault, G. Perez, R. Bouaziz, *C. r. hebd. séances Acad. sci. serie C*. **278**(4), 251 (1974).
26. B. Monnaye, Li_2MGeO_4 series (M = Mg Ca, Fe, Co, Ni Zn, Cd) – structural relationship between mixed germinate, *Rev. Chim. Miner.,* **13**(5), 422 (1976).
27. N. K. Nakayama, K. Takahashi, K. Fujiwara, A. Nakatsuka, M. Isobe, Y. Ueda, *TMRS-J*, **38**(3), 419 (2013). https://doi.org/10.14723/tmrsj.38.419.
28. A. C. Larson, R. B. Von Dreele, General Structure Analysis System (GSAS), Report LAUR, Los Alamos National Laboratory. 86 (2000). https://www.ncnr.nist.gov/xtal/software/gsas.html.
29. B. H. Toby, EXPGUI, a graphical user interface for GSAS, *J. Appl. Crystallogr.*, **34**, 210 (2001). https://doi.org/10.1107/S0021889801002242.
30. T. Roisnel, J. Rodriguez-Carvajal, WinPLOTR, version May 2000: Materials Science Forum, in: Proceedings of the 7th European Powder Diffraction Conference, Barcelona, Spain, 20–23 May 2000, R. Delhez, E. J. Mittenmeijer (eds.), Scitec Publications, Ltd., Baech, Switzerland, 2000, p. 118.
31. K. Momma, F. Izumi, VESTA 3 for three-dimensional visualization of crystal, volumetric and morphology data, *J. Appl. Crystallogr.*, **44**, 1272 (2011). https://doi.org/10.1107/S0021889811038970.
32. E. Plattner, H. Völlenke, A. Wittmann, *Monatsh. Chem.*, **107**(4), 921 (1976). https://doi.org/10.1007/BF00904478.
33. H. Völlenkle, *Z. Kristallogr. – Cryst. Mater.*, **154**(1–4), 77 (1981). https://doi.org/10.1524/zkri.1981.154.14.77.
34. P. G. Bruce, A. R. West, *J. Solid State Chem.*, **44**(3), 354 (1982). https://doi.org/10.1016/0022-4596(82)90383-8.